RSC Advances

PAPER

View Article Online
View Journal | View Issue

Cite this: *RSC Adv.*, 2019, **9**, 853

A DFT study on nanocones, nanotubes (4,0), nanosheets and fullerene C_{60} as anodes in Mg-ion batteries†

Esmail Vessally, *[ab] Ibon Alkorta, *[b] Sheida Ahmadi,[a] Robab Mohammadi[a] and Akram Hosseinian [c]

Received 16th July 2018
Accepted 14th December 2018

DOI: 10.1039/c8ra06031b

rsc.li/rsc-advances

In this article, we studied the interactions between Mg atom and Mg^{2+} ion and four nanostructures, including a nanocone, nanotube (4,0), nanosheet, and C_{60} nanocage, to obtain the cell voltages (*V*) for Mg-ion batteries (MIBs). Total energy, geometry optimization, frontier molecular orbital (FMO) and density of states (DOS) analyses have been performed using the ωB97XD level of theory and the 6-31G(d) basis set. The DFT calculations clarified that the changes in energy adsorption between Mg^{2+} ion and the nanostructures, E_{ad}, are in the order tube > cone > sheet > cage. However, V_{cell} for the nanocone is the highest. The changes in V_{cell} of the MIBs are in the order cone > tube > sheet > cage. This study theoretically considers the possibilities of Mg as an anode in batteries due to its high V_{cell} values.

1 Introduction

Secondary batteries or rechargeable batteries are very important for producing electricity in various devices. In addition to wet batteries, such as lead-acid batteries, which contain liquid electrolyte in an unsealed container, dry batteries, such as zinc–carbon, nickel–cadmium, nickel–zinc and lithium-ion batteries, are well-known and have attracted much attention due to the facility of their transportation. Some dry batteries have disadvantages, including heavy metals, which are significant environmental pollutants due to their toxicity and transport issues.

Lithium (Li) is a suitable anode metal for rechargeable batteries because of its low density, high specific capacity, and lowest electrochemical potential in the periodic table.[1] Regarding the battery systems in Li batteries, the movement of Li^+ ions through the electrolyte and electrons through the external electrical circuit to the cathode lead to a suitable battery system. Therefore, we have designed a simple model system in the present work which can reveal preliminary knowledge about the possibilities of electron transfer. This model can reveal some details about the electron transfer process which have not been thoroughly studied in experimental research on Li–CO_2 batteries. We hope that the computational data reported in the present work will motivate experimental researchers to investigate this simple model system and compare their experimental results.

Li-ion batteries have some disadvantages, such as low-voltage energy storage, high cost and environmental issues.[1] Sodium-ion batteries (SIBs)[2] and magnesium-ion batteries (MIBs)[3–5] have been suggested as useful alternatives because of their low cost and high availability. However, SIBs have high gravimetry; thus, they are not suitable for vehicles and electronic instruments.[3] Rechargeable Mg-ion batteries are a promising candidate technology for future electrical energy storage because of the abundance of magnesium and its divalent character, which leads to strong interactions of Mg^{2+}.[6]

There are a few reports in the literature of theoretical or experimental studies on MIBs. Matsui and coworkers experimentally studied α-MnO_2 as a cathode material for rechargeable Mg batteries. Their studies showed that α-MnO_2 is a promising candidate as a cathode material for rechargeable Mg batteries if its capacity retention can be significantly improved.[7] J. Chen and co-workers reported that TiS_2 nanotubes can be used as cathode materials in rechargeable Mg-ion batteries, indicating important advantages in terms of environmental considerations, safety and relatively high capacity.[8]

A few theoretical studies have been carried out on potential Mg-ion batteries (MIBs). In 2018, J. Sun and co-workers[9] reported density functional theory calculations for the evaluation of phosphorene as a potential anode material for magnesium batteries. They estimated that the average voltage of Mg adsorption in phosphorene is 0.833 V, which is suitable for its application as an anode in MIBs. A. O. Pereira and co-workers reported a first-principles investigation of transition metal dichalcogenide nanotubes for Li and Mg ion battery

[a]*Department of Chemistry, Payame Noor University, Tehran, Iran. E-mail: vessally@yahoo.com*

[b]*Instituto de Química Medica (CSIC), Juan de la Cierva, 3, Madrid 28006, Spain. E-mail: ibon@iqm.csic.es*

[c]*School of Engineering Science, College of Engineering, University of Tehran, P. O. Box 11365-4563, Tehran, Iran*

† Electronic supplementary information (ESI) available. See DOI: 10.1039/c8ra06031b

applications.[10] They investigated the adsorption and diffusion properties of Li and Mg in MoS_2 and WS_2 nanotubes. They found that the Mg intercalation in WS_2 and MoS_2 nanotubes showed remarkable diffusion properties in comparison to Li insertion.[10]

Recently, various nanoparticles have been studied for application in the electronics, optics and sensor fields.[11–13] It has been indicated that some nanoparticles are suitable for use in ion batteries.[14–17] Nanotubes, nanosheets and fullerenes have been studied as anode electrodes for lithium-ion batteries (LIBs) and SIBs.[14,18] Some inorganic nanosheets, such as ZnO, SiC and MgO, have been reported as anodes in ion batteries.[14,19,20]

Our goal in this work is to study the use of carbon nanostructures with different shapes as anodes in Mg-ion batteries. Different shapes of nanostructures lead to different interactions between Mg^{2+}/Mg and the nanostructures, which causes variations in the cell voltage. We investigated the interactions between Mg atom and Mg^{2+} ion and four nanostructures, including a nanocone, nanotube (4,0), nanosheet, and C_{60} nanocage (Fig. 1). The aim of this work was to obtain the cell voltages (V) of Mg-ion batteries based on the four nanostructures (Table 1).

2 Computational methods

Total energy, geometry optimization, Frontier molecular orbital (FMO) and density of states (DOS) analyses were carried out at the ωB97XD level of theory using the 6-31G(d) basis set.[21] The ωB97XD method has a higher % HF exchange, which predicts E_g more accurately than other general DFT methods, such as B3LYP.[22] All calculations were performed using the G09 program.[23] In the optimization process, all atoms were optimized, and none of the atoms were fixed. The vibrational frequencies were calculated for our systems. All the structures were true minima on the potential energy surface. The first vibration wavelength numbers of the nanostructures and their complexes are presented in Table 2; the results indicate that no imaginary frequencies were found.

The wB97XD includes a dispersion term proposed by Grimme to properly describe weak interactions.[24] The molecular formulas of the studied nanostructures are nanocone, $C_{80}H_{20}$; nanotube, $C_{56}H_8$; nanosheet, $C_{54}H_{18}$; and nanocage, C_{60}. Hydrogen atoms were used to cap the boundary carbon atoms of the nanostructures.

The natural bond orbitals (NBO) of the Mg^{2+}/Mg-nanocone complex were calculated for charge and hybridization analysis.

The Mg and Mg^+ adsorption energies were computed by the following equation:

$$E_{ad} = E_{complex} - E_{nanostructure} - E_{Mg/Mg^{2+}} + E_{BSSE} \quad (1)$$

where $E_{nanostructure}$ is the energy of the nanostructure, including the nanocone, nanotube, nanosheet and nanocage. $E_{complex}$ is the energy of each nanostructure on which Mg or Mg^{2+} was adsorbed over the surface. E_{BSSE} relates to the basis set superposition error, which was calculated by the counterpoise method of Boys and Bernardi[25] at the optimized geometry using the keyword "counterpoise". The non-BSSE corrected energies are also shown in Table 1 to indicate the importance of the BSSE correction. According to the results given in Table 1, the BSSE

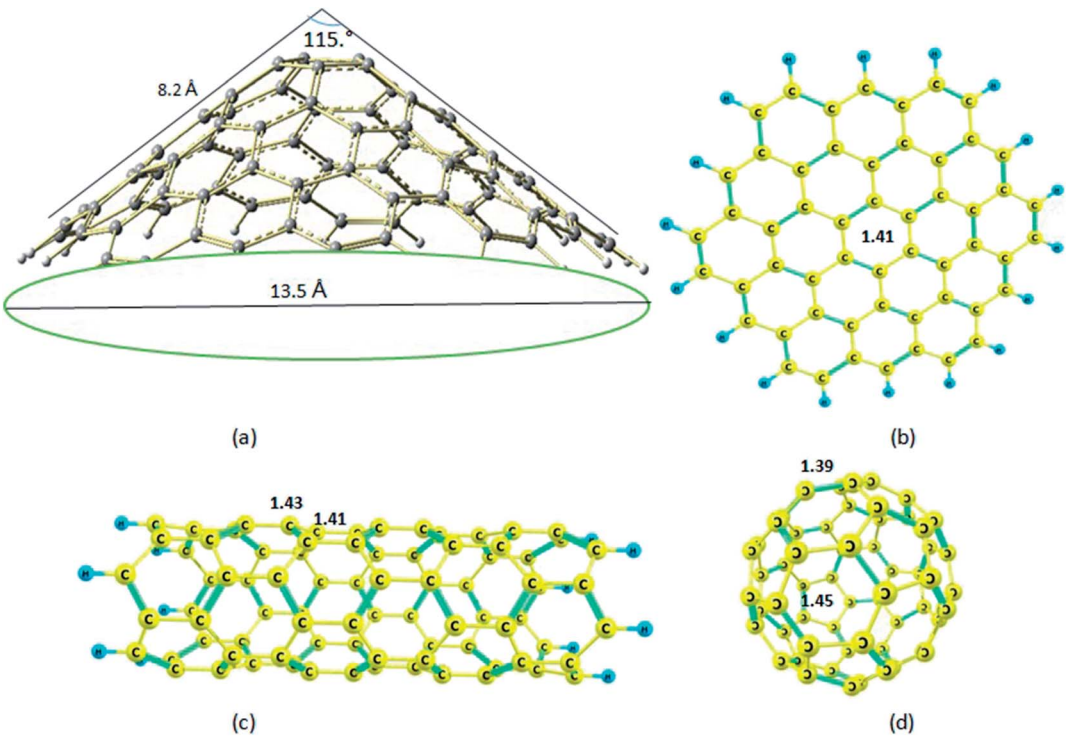

Fig. 1 Optimized molecular structures of the (a) nanocone; (b) nanosheet; (c) nanotube; (d) nanocage.

Table 1 The adsorption energies of atomic Mg and Mg^{2+} (E_{ad}, kcal mol^{-1}) on the different nanostructures[a]

Nanostructure	E_{ad} non-BSSE	E_{ad} BSSE	E_{HOMO}	E_{LUMO}	E_g	% ΔE_g	ΔE_{cell}	V_{cell}
Cone	—	—	−6.5	−1.3	5.2	—	−191.2	−4.1
Cone/Mg^{2+}	−194.9 (−192.1)[b]	−192.8 (−190.2)[b]	−10.6 (−10.6)	−7.4 (−7.4)	3.2 (3.3)	−38.5 (−37.1)	(−188.0)	(−4.1)
Cone/Mg	−2.6 (−3.1)	−1.7 (−2.2)	−6.4 (−6.5)	−1.4 (−1.4)	5.0 (5.1)	−3.4 (−2.0)		
Tube	—	—	−6.4	−2.2	4.2	—	−177.2	−3.8
Tube/Mg^{2+}	−239.6	−236.8	−11.8	−8.0	3.8	−8.5		
Tube/Mg	−62.7	−59.5	−6.0	−2.1	3.8	−8.7		
Sheet	—	—	−6.4	−0.8	5.7	—	−173.4	−3.8
Sheet/Mg^{2+}	−177.6	−176.1	−11.7	−8.0	3.7	−34.7		
Sheet/Mg	−3.5	−2.7	−6.4	−0.8	5.6	−1.7		
C_{60}	—	—	−7.8	−1.8	6.0	—	−142.6	−3.1
C_{60}/Mg^{2+}	−145.7	−143.6	−13.3	−8.7	4.6	−23.2	(−141.4)	(−3.1)
	(−144.7)	(−142.7)	(−13.4)	(−8.7)	(4.8)	(−21.3)		
C_{60}/Mg	−1.8	−1.1	−6.9	−1.8	5.1	−16.1		
	(−2.2)	(−1.2)	(−6.7)	(−1.9)	(5.0)	(−17.1)		

[a] Energies of the HOMO, LUMO, and HOMO–LUMO gap (E_g) are in eV. ΔE_g indicates the change in E_g of the nanostructure after Mg/Mg^{2+} adsorption. The total energy changes (ΔE_{cell}, kcal mol^{-1}) and cell voltages (V) of the nanostructure-based Mg-ion batteries are shown. [b] Amounts in parenthesis are for interactions over the six-membered ring.

correction is quite small (approx. 1 kcal mol^{-1}), which implies that BSSE does not play an important role. Therefore, small BSSE corrections for a moderate 6-31G(d) basis set may be related to a single point calculation to obtain the BSSE corrections.

The HOMO–LUMO energy gap (E_g) is computed as:

$$E_g = E_{LUMO} - E_{HOMO} \quad (2)$$

where E_{LUMO} and E_{HOMO} are the energies of the HOMO and LUMO levels. The change in E_g was computed as follows:

$$\Delta E_g = [(E_{g2} - E_{g1})/E_{g1}] \times 100 \quad (3)$$

where E_{g1} and E_{g2} are the pristine value and the complex value, respectively. This parameter indicates the electronic sensitivity of the nanostructure to Mg/Mg^{2+} adsorption. The GaussSum program was used to calculate the DOS plots.[26]

3 Results and discussion

For each nanostructure [the nanocone, nanotube (4,0), nanosheet or C_{60} nanocage], the physical parameters of the isolated nanostructures and their interaction energies with Mg atom or Mg^{2+} ion were considered first. Finally, the cell voltages (V) of the four nanostructure-based Mg-ion batteries (MIBs) were calculated and discussed.

We examined all the regions at the top of the pentagon or hexagon rings, especially the top carbon atoms, for possible interactions with ionic or neutral Mg. The global minima for interactions between the metal and cone were obtained when Mg was located in the top middle of the pentagon or hexagon ring.

3.1 Adsorption of Mg/Mg^{2+} over the nanocone

The structure of the nanocone, with a five-membered ring at its tip and six-membered rings connected to the five-membered

Table 2 Gibbs free energies (G), relative free energies (ΔG), energy differences between the nanostructure-Mg^{2+} and nanostructure-Mg complexes ($\Delta\Delta G$), relative entropy terms ($T\Delta S$), and first vibration wavelength numbers of the nanostructures and their complexes with atomic Mg and Mg^{2+}

Nanostructure	ΔG kcal mol^{-1}	$\Delta\Delta G$ kcal mol^{-1}	$T\Delta S$ kcal mol^{-1}	ν_1^{-1} cm^{-1}
Cone	—		—	36.7
Cone/Mg^{2+}	−195.6	−198.5	−16.4	36.4
Cone/Mg	2.9		−16.4	17.8
Tube	—		—	100.4
Tube/Mg^{2+}	−239.2	−186.6	−17.0	53.0
Tube/Mg	−52.5		−17.1	38.0
Sheet	—		—	40.7
Sheet/Mg^{2+}	−178.3	−180.5	−21.4	41.4
Sheet/Mg	2.2		−21.4	19.7
C_{60}	—			269.9
C_{60}/Mg^{2+}	−145.8	−148.6	−15.4	150.4
C_{60}/Mg	2.9		−15.5	10.7

ring, is shown in Fig. 1. A detailed description of the geometrical parameters of the carbon nanocone is presented in Fig. 1. The opening angle of the cone is about 115°. The length and diameter of the cone are 8.2 and 13.5 Å, respectively.[27] The bond length of the C–C bonds of the nanocone in the five-membered ring is 1.42 Å, which is consistent with a previous article.[16] The HOMO and LUMO energies are −6.51 and −1.33 eV, respectively; thus, the HOMO–LUMO gap energy is 5.18 eV (Table 1). In order to study the adsorption behavior of Mg^{2+}/Mg on the nanocone, it was necessary to examine all possibilities of interaction between Mg^{2+}/Mg and the five and six-membered rings of the nanocone.

3.1.1 Adsorption of Mg/Mg^{2+} over the nanocone on the five-membered ring. The interactions of Mg^{2+} ion and Mg atom over the five-membered ring show distances of 1.82 and 3.45 Å to the plane of the ring (Fig. 2), respectively. This indicates a strong interaction between the nanocone and Mg^{2+} due to the high charge concentration of the Mg^{2+} ion, while the interaction with the neutral Mg atom is weak. The adsorption energy, E_{ad}, of the Mg^{2+} ion on the nanocone is −192.8 kcal mol^{-1}; this is larger than that of the Mg atom (−1.7 kcal mol^{-1}) (Table 1).

The formation of a complex with Mg^{2+} decreases the energies (more negative) of both the HOMO and LUMO levels (Fig. 3). However, the shift of the LUMO level is more significant, from −1.33 eV in the isolated molecule to −7.43 eV in the Mg^{2+} nanocone complex (Table 1). Therefore, E_g of the nanocone decreased from 5.18 in the pristine nanocone to 3.18 in the Mg^{2+}-nanocone complex.

These large changes in E_g are attributed to large changes in the size and shape of the LUMO. The LUMO in the Mg^{2+}-nanocone complex lies on the Mg^{2+} cation. The changes in the HOMO, LUMO and E_g are illustrated in Fig. 4 by density of states (DOS) diagrams. The plot of the partial density of states (PDOS, Fig. 5) clearly indicates that a new level produced at the E_g gap of the pristine nanocone mostly arises from the Mg^{2+} cation, which leads to a decrease in E_g of the Mg^{2+}-nanocone complex.

In contrast, the Mg atom does not significantly change the HOMO or LUMO levels or, consequently, the E_g value. The Mg atom slightly decreases the LUMO level and increases the HOMO level.

The NBO analysis shows a charge transfer of 0.19*e* from the nanocone to the Mg^{2+} cation. This value is higher than that of an analogous system with Na^+.[14] In the neutral complex, only 0.004*e* are transferred from the Mg atom to the nanocone, which is less than the corresponding complex with Na atom.

The hybridization of the carbon atoms in the five-membered ring in the center of the nanocone is $sp^{2.11}$. After the adsorption of Mg^{2+}, the hybridization of the carbon atoms changes to $sp^{2.21}$. The DFT calculations indicate that the p character of the carbon atoms in the five-membered ring increases with adsorption of Mg^{2+} because these carbon atoms tend to interact with the Mg^{2+} cation. Strong interactions between carbon atoms in the five-membered ring and Mg^{2+} lead to an increment of the p character of the carbon atoms and, consequently, to an increment of the bond length from 1.419 in the pristine nanocone to 1.433 Å in the Mg^{2+}-nanocone complex.

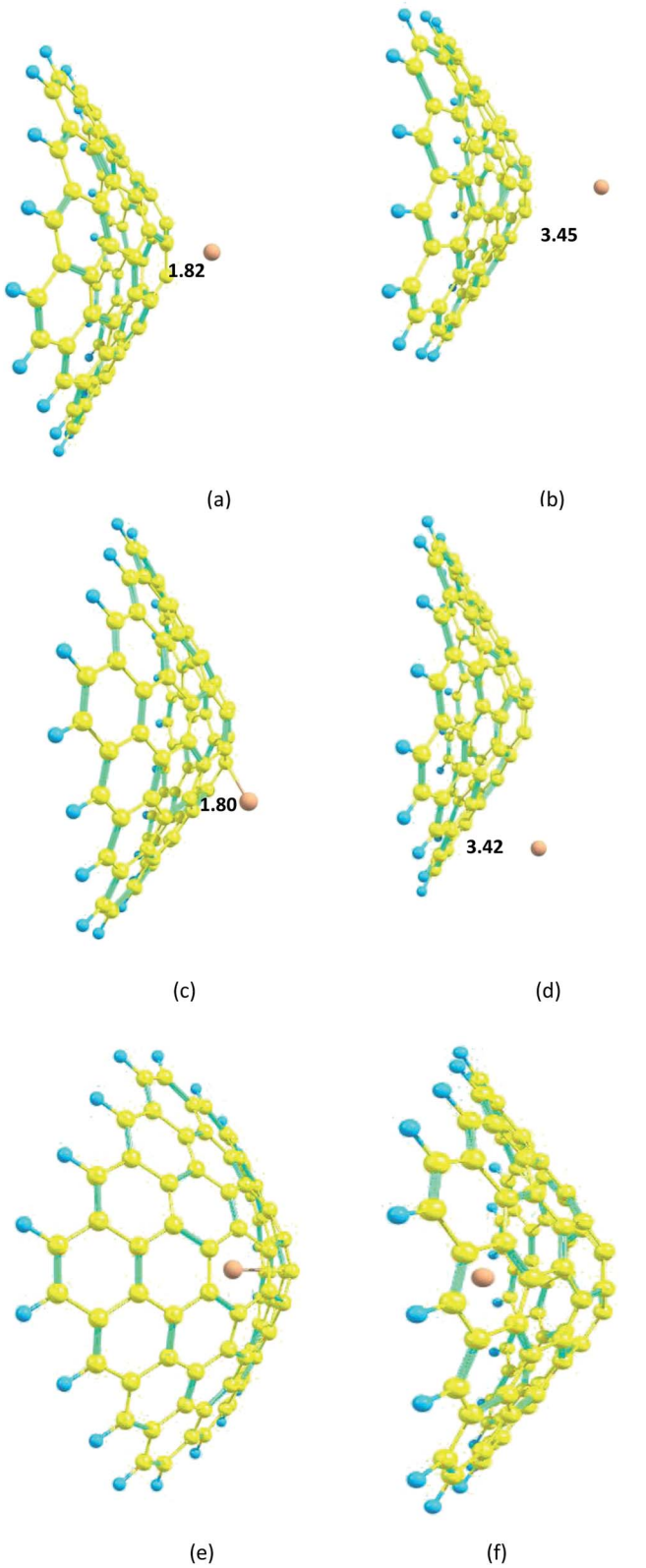

Fig. 2 Optimized structures of the Mg^{2+} and Mg-nanocone complexes. (a) Mg^{2+} over the five-membered ring; (b) Mg over the five-membered ring; (c) Mg^{2+} over the six-membered ring; (d) Mg over the six-membered ring; (e) Mg^{2+} inside the nanocone; (f) Mg inside the nanocone. Distances are in Å.

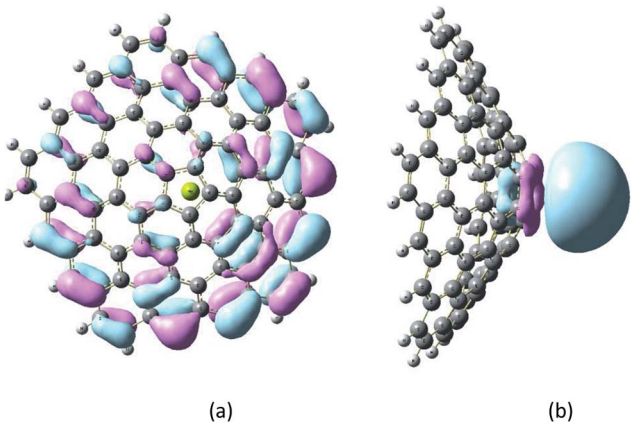

(a) (b)

Fig. 3 HOMO and LUMO diagrams of the Mg^{2+}-nanocone complex: (a) HOMO; (b) LUMO.

The electron density (ρ) and the Laplacian of the electron density ($\nabla^2\rho$) are two significant criteria to evaluate the strength and character of a chemical bond.[32,33] In this regard, we investigated ρ and $\nabla^2\rho$ for the C–C and Mg–C chemical bonds in the five-membered ring based on AIM theory,[28] as shown in Fig. 6. According to our results, the magnitude of ρ (0.300 a.u.) and the negative sign of $\nabla^2\rho$ (−0.792 a.u.) for the C–C chemical bonds in the pristine nanocone and the magnitude of ρ (0.291 a.u.) and the negative sign of $\nabla^2\rho$ (−0.736 a.u.) for the Mg^{2+}-nanocone complex reflect the covalent character of the C–C chemical bonds, while the magnitude decreases for the Mg^{2+}-nanocone complex due to interactions between the five-membered carbon atoms and Mg^{2+}. In contrast to the C–C chemical bonds, the character of the Mg^{2+}–C chemical bonds should be non-covalent due to the small value of ρ (0.032 a.u.) and the positive sign of $\nabla^2\rho$ (0.168 a.u.).

3.1.2 Adsorption of Mg/Mg^{2+} over the nanocone on the six-membered ring. Mg^{2+} ion and Mg atom can locate over the six-membered ring at distances of 1.80 and 3.42 Å, respectively. The adsorption energy, E_{ad}, of Mg^{2+} ion on the nanocone is −190.2 kcal mol^{-1}, and that of the neutral Mg atom is −2.2 kcal mol^{-1} (Table 1). Thus, the interaction of Mg^{2+} with the nanocone occurs preferentially in the five-membered ring, while that of Mg atom occurs in the six-membered ring.

As in the case of the adsorption of Mg^{2+} on the five-membered ring, both the HOMO and LUMO levels change to lower energies, and the effect on the LUMO is greater than on the HOMO. The LUMO level changes from −1.33 eV in the pristine nanocone to −7.37 eV in the Mg^{2+}-nanocone complex (Table 1). Therefore, E_g of the nanocone decreased from 5.18 in the pristine nanocone to 3.26 in the Mg^{2+}-nanocone complex. Based on the adsorption energy, E_{ad}, and the HOMO–LUMO gap, E_g, we may conclude that the adsorption of Mg^{2+} over the five-membered ring in the nanocone is more suitable for Mg-ion batteries than adsorption over the six-membered rings.

In the case of the nanocone, adsorption can occur on concave or convex surfaces (Fig. 2e and f). It is important and interesting to compare the calculated data for both cases. The interaction between Mg^{2+} and the nanocone on a concave surface is greater (−1.1 kcal mol^{-1}) than on a convex surface. However, the stronger interaction between Mg and the nanocone on a concave surface (−4.0 kcal mol^{-1}) with respect to a convex surface leads to low ΔE_{cell} and V_{cell} values.

3.2 Adsorption of Mg/Mg^{2+} over the nanotube (4,0)

The carbon nanotube (4,0) with a zigzag configuration is shown in Fig. 7; its terminal carbons are capped with hydrogen atoms. There are two types of C–C bonds in the nanotube, whose bond lengths are 1.41 and 1.43 Å; this shows that the two bonds are different and form a boat structure. The HOMO and LUMO energies of the nanotube are −6.42 and −2.23 eV, respectively; thus, the HOMO–LUMO gap energy is 4.19 eV. The Mg^{2+} ion and Mg atom interact with the six-membered ring; after optimization, the distances between the Mg^{2+} ion and Mg atom and the plane of the nanotube become 1.61 and 1.68 Å, respectively, indicating strong interactions between the nanotube and both Mg^{2+} and Mg. The surprisingly strong interactions for both

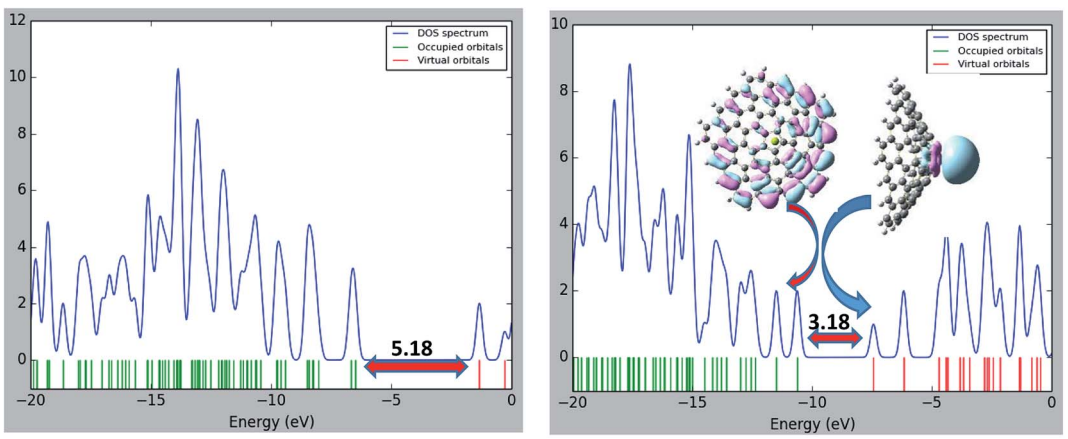

(a) (b)

Fig. 4 Density of states (DOS) plots of (a) the pristine nanocone; (b) the Mg^{+2}-nanocone complex. The E_g units are in eV.

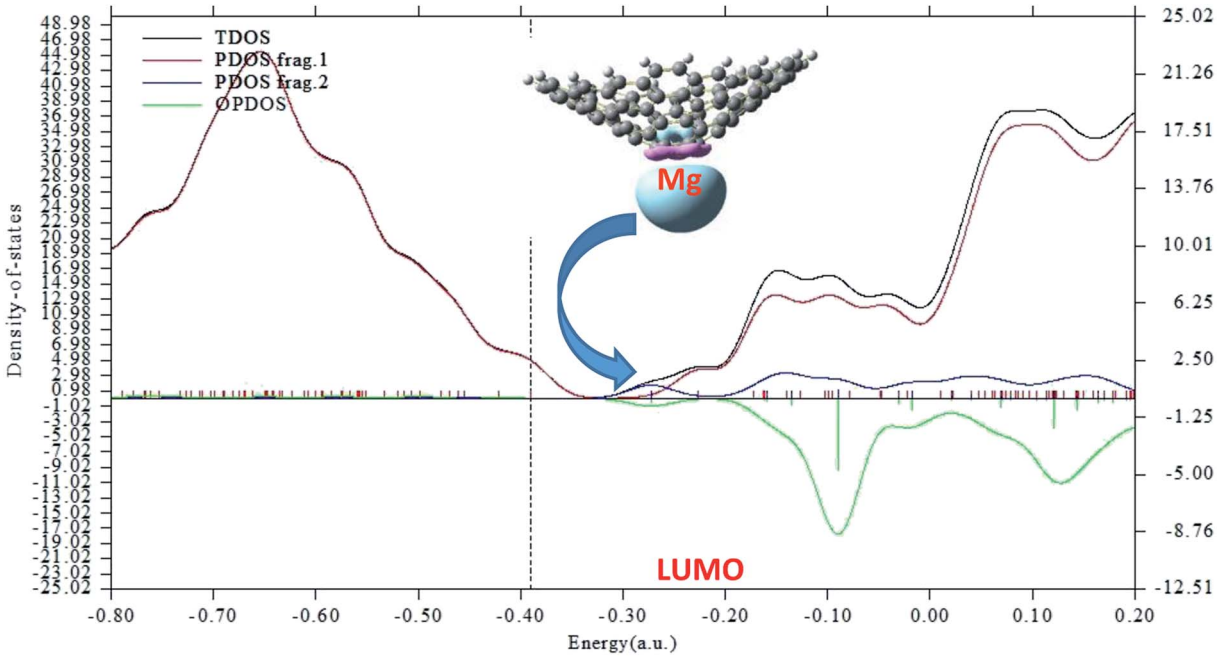

Fig. 5 Partial density of states (PDOS) plot of the Mg^{2+}-nanocone complex. The red and blue lines indicate the nanocone and Mg^{2+}, respectively. The LUMO profile of this complex is also depicted.

Mg^{2+} ion and Mg atom can be attributed to the boat conformation of the rings in the nanotube, which act as molecular clips. These results resemble the ionic structure described for a C_6H_6 : Li complex.[30]

The adsorption energy, E_{ad}, of Mg^{2+} ion on the nanotube is -236.8 kcal mol^{-1}, and that of Mg atom is -59.5 kcal mol^{-1} (Table 1). Our results indicate that the adsorption energies, E_{ad}, of both Mg^{2+} ion and Mg atom on the nanotube are stronger than on the nanocone.

Both the HOMO and LUMO levels of the Mg^{2+} and Mg-complexes change to lower energies (more negative), where the shift of the Mg^{2+}-complex is greater. However, the E_g of the nanotube slightly decreased from 4.19 in the pristine nanotube to 3.84 in the Mg^{2+}-nanotube complex, which indicates a low sensing effect with absorption of Mg^{2+} on the nanotube. The ΔE_g of the Mg^{2+}-nanotube complex is -8.5, which is smaller in absolute value than that of the Mg^{2+}-nanocone complex (-38.5).

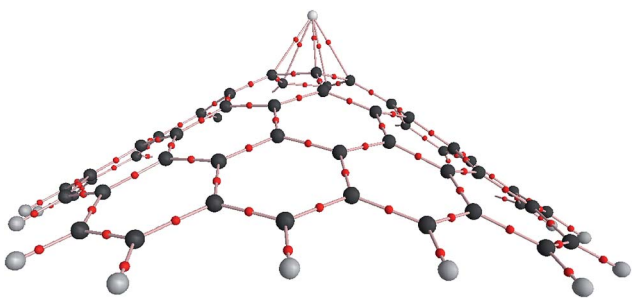

Fig. 6 Molecular graph of the Mg^{2+}-nanocone complex using AIM analysis at the wB97XD/6-31G(d) level.

3.3 Adsorption of Mg/Mg^{2+} over the nanosheet

The carbon nanosheet model used in the calculation and formed only with six-membered rings is shown in Fig. 1. The bond length of the C–C bond in the nanosheet is 1.41 Å, which is consistent with previous work.[14] The HOMO and LUMO energies are -6.44 and -0.76 eV, respectively; thus, the HOMO–LUMO gap energy is 5.69 eV. The Mg^{2+} ion and Mg atom interact over the six-membered ring with distances 1.86 and 3.35 Å from the plane of the nanosheet, respectively (Fig. 8); this indicates strong interactions between Mg^{2+} and the nanosheet. The E_{ad} of

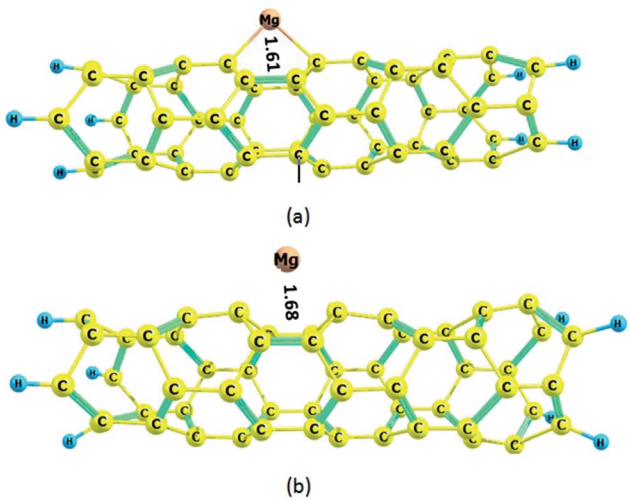

Fig. 7 Optimized structures of the Mg^{2+} and Mg-nanotube complexes: (a) Mg^{2+}-nanotube complex, (b) Mg-nanotube complex. Distances are in Å.

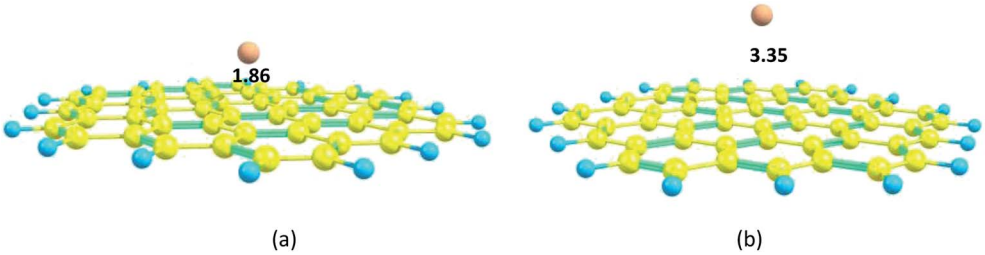

Fig. 8 Optimized structures of the Mg^{2+} and Mg-nanosheet complexes: (a) Mg^{2+}-nanosheet complex, (b) Mg-nanosheet complex. Distances are in Å.

the Mg^{2+} ion on the nanosheet is −176.1 kcal mol^{-1} and E_{ad} for the Mg atom is −2.7 kcal mol^{-1} (Table 1).

Both the HOMO and LUMO levels change to lower energies, where the shift of the LUMO level to a lower energy is greater. The LUMO level changed from −0.76 eV in the nanosheet to −7.99 eV in the Mg^{2+}-nanosheet complex (Table 1). Therefore, E_g of the nanosheet decreased from 5.69 in the pristine nanosheet to 3.71 in the Mg^{2+}-nanosheet complex, which indicates that the nanosheet interacts sensitively with Mg^{2+} ion. The ΔE_g of the Mg^{2+}-nanosheet complex (−34.7) has a larger absolute value than that of the Mg^{2+}-nanotube complex (−8.5).

3.4 Adsorption of Mg/Mg^{2+} over the nanocage

The carbon nanocage, C_{60}, shows five-membered and six-membered rings, as illustrated in Fig. 1. The bond length of the C–C bonds in the five-membered ring of the nanocage is 1.45 Å, which is longer than that in the six-membered ring (1.39 Å). The HOMO and LUMO energies for the isolated nanocage are −7.83 and −1.79 eV, respectively; thus, the HOMO–LUMO gap energy is 6.04 eV. The E_g values for the four nanostructures considered here are in the order cage > sheet > cone > tube, which indicates that the nanocage can have high stability and low interaction energy with Mg^{2+}. Because there are two interaction sites in the cage, it was necessary to consider two types of adsorption sites between Mg^{2+}/Mg and the nanocage over both the five and six-membered rings.

The optimized distances of the Mg^{2+} ion and Mg atom located over the five-membered ring are 1.87 and 3.59 Å, respectively; meanwhile, the distances of Mg^{2+} ion and Mg atom over the six-membered ring are 1.88 and 3.60 Å, respectively (Fig. 9).

The adsorption energy, E_{ad}, of Mg^{2+} ion on the five-membered ring of the nanocage is −143.6 kcal mol^{-1}, which is larger than that of Mg atom (−1.1 kcal mol^{-1}); meanwhile, the adsorption energies, E_{ad}, of Mg^{2+} ion and Mg atom on the six-membered ring are −142.7 and −1.2 kcal mol^{-1}, respectively (Table 1). Thus, the E_{ad} of the Mg^{2+}-cage has the lowest adsorption energy, and E_{ad} changes in the order tube > cone > sheet > cage.

Both the HOMO and LUMO levels of the Mg^{2+}-cage complex transfer to lower energies; the shift of the LUMO level to a lower energy is greater. The LUMO level changed from −1.79 eV to −8.69 eV (Table 1). Therefore, E_g of the nanocage decreased from 6.04 to 4.63 in the Mg^{2+}-nanocage complex, and the ΔE_g of the Mg^{2+}-nanostructure became −23.2.

The Gibbs free energies (G), relative free energies (ΔG), energy differences between the nanostructure-Mg^{2+} and nanostructure-Mg complexes ($\Delta\Delta G$), and entropy terms ($T\Delta S$) are shown in Table 2. The more negative values of $\Delta\Delta G_{ad}$ indicate that adsorption of Mg^{2+}/Mg on the nanostructures can proceed spontaneously. The adsorptions of Mg^{2+} on all the nanostructures and Mg on the nanotube proceed spontaneously, while the adsorptions of neutral Mg on the cone, sheet and cage do not proceed spontaneously.

The value of $T\Delta S_{ad}$ decreases during the adsorption process, which is due to a decrease of the degrees of freedom for the nanostructure-Mg^{2+}/Mg complexes. The entropy terms ($T\Delta S$) are identical for both the nanostructure/Mg^{2+} and nanostructure/Mg complexes. The $T\Delta S$ values for both the cone/Mg^{2+} and cone/Mg species are 16.4 kcal mol^{-1}, which may be negligible compared to the ΔG value of −195.6 kcal mol^{-1}.

The calculated adsorption energies, E_{ad}, are consistent with the relative free energies, ΔG (Tables 1 and 2). The highest ΔG values for the nanostructure-Mg^{2+} and -Mg complexes correspond to the nanocone and nanotube, respectively. The energy differences between the nanostructure-Mg^{2+} and nanostructure-Mg complexes, $\Delta\Delta G$, are consistent with ΔE_{cell} (Tables 1 and 2).

3.5 Comparison of the nanostructures in Mg^{2+}-ion batteries (MIBs)

Four types of nanostructures were suggested as anodes for MIBs. The formal reactions in the anode and cathode are as follows:[29]

$$\text{Anode: Mg-nanostructure} \leftrightarrow \text{Mg}^{2+}\text{-nanostructure} + 2e^- \quad (4)$$

This reaction can be divided into several formal reactions that are presented below:

$$\text{Cathode: } Mg^{2+} + 2e^- \leftrightarrow Mg \quad (5)$$

The total reaction of the cell can be defined as:

$$Mg^{2+} + \text{Mg-nanostructure} \leftrightarrow Mg^{2+}\text{-nanostructure} + Mg + \Delta G_{cell} \quad (6)$$

This equation is related to the binding energy on one hand and to the ionization potential of Mg on the other hand.

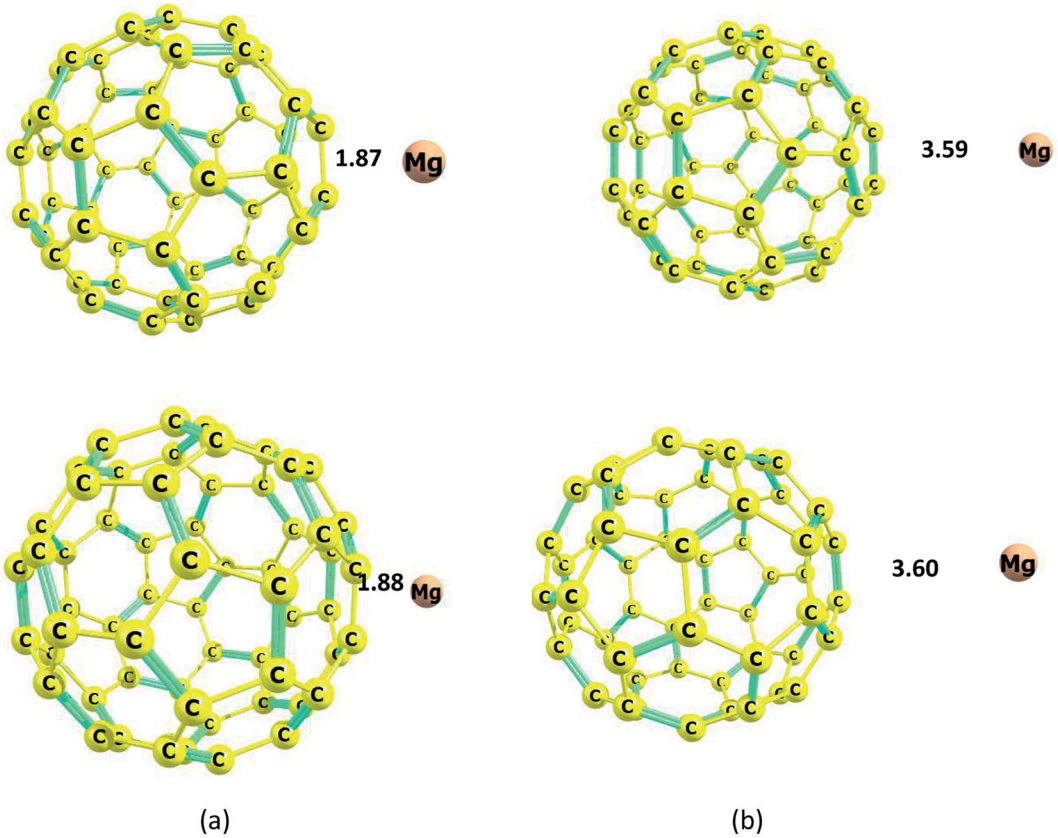

Fig. 9 Optimized structures of the Mg^{2+} and Mg-nanocage complexes. (a) Mg^{2+}-nanocage complex, (b) Mg-nanocage complex. Distances are in Å.

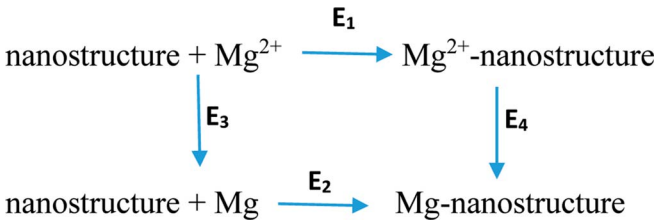

where E_1 and E_2 are the binding energies and E_3 and E_4 are the ionization potentials, which can be related with the following equations: $E_1 + E_4 = E_3 + E_2$ or $E_1 - E_2 = E_3 - E_4$.

The Nernst equation is used to obtain the cell voltage (V_{cell}) as follows:

$$V_{cell} = -\Delta G_{cell}/zF \quad (7)$$

where F and z are the Faraday constant (96 500 C mol^{-1}) and the charge of Mg^{2+} ($z = 2$, the cation in the electrolyte), respectively. The ΔG_{cell} is the Gibbs free energy difference of the total reaction of the cell. For DFT calculations at 0 K, it can be presented as:

$$\Delta G_{cell} = \Delta E_{cell} + P\Delta V - T\Delta S \quad (8)$$

In previous reports, we confirmed that the volume and entropy contributions to V_{cell} are very small (<0.01 V).[29] Therefore, V_{cell} for the Mg^{2+}- or Mg-nanostructure complexes can be determined by calculating the internal energy change (ΔE) from eqn (6) and (8) as follows:

$$\Delta E_{cell} \sim \Delta G_{cell} = E_{Mg} + E_{Mg^{(2+)}\text{-nanostructure}} - E_{Mg^{(2+)}} - E_{Mg\text{-nanostructure}} \quad (9)$$

Eqn (9) indicates that the simultaneous strong interaction between Mg^{2+} and the nanostructure and the weak interaction between Mg atom and the nanostructure affords a more negative and higher ΔE_{cell}. In conclusion, the strong adsorption of Mg^{2+} and the weak adsorption of Mg on the nanostructure lead to a high V_{cell} (Table 1). ΔE_{cell} and V_{cell} were calculated for the four nanostructures and are presented in Table 1 and illustrated in Fig. 10. The ΔE_{cell} and V_{cell} values for the four nanostructures in MIBs changed in the same order: cone > tube > sheet > cage. The largest ΔE_{cell} and V_{cell} values are −191.2 kcal mol^{-1} and 4.1 V, respectively, which are related to the nanocone. ΔE_{cell} and V_{cell} for the nanotube in a MIB are −177.2 kcal mol^{-1} and 3.8 V, respectively, which are lower than the values for the nanocone. However, V_{cell} of the nanotube (3.8 V) is larger than that reported for Li-ion batteries (1.45 V) by Gao *et al.*,[31] which was calculated at the B3LYP/6-31G(d) level of theory. The strongest interaction between Mg^{2+} and the nanotube implies that the MIB-nanotube will have the largest V_{cell} value; meanwhile, the strong interaction between the Mg atom and the nanotube led to a decrease in the V_{cell} value. The lowest V_{cell} value belongs to

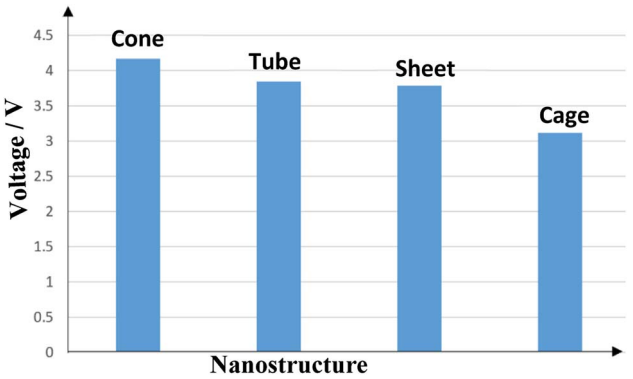

Fig. 10 Diagram of the cell voltages of the different nanostructures as anodes in Mg ion batteries (MIBs).

the MIB-nanocage due to the weakest interaction between Mg^{2+} and the nanocage, which was confirmed by the high E_g of the nanocage; this is probably due to the spherical structure of fullerene 60. In general, the V_{cell} values for the MIBs-nanostructures range from −3.1 to −4.1 V; thus, these nanostructures are promising candidates for application as anodes in the manufacture of MIBs. We can conclude that the advantages of Mg, including its low cost, availability and high V_{cell} value, will encourage the battery scientists to study these MIBs-nanostructures after overcoming their technical issues.

All calculations were performed in the gas phase. Certainly, the study of solvent effects on these systems would be useful to further support the experimental data.

4 Conclusions

In this work, the adsorption of Mg^{2+} and Mg on nanostructures, including a nanocone, nanotube (4,0), nanosheet, and C_{60} nanocage, was studied to scrutinize their possible application as anodes of MIBs. The interactions between Mg^{2+} and the surfaces of the nanostructures are clearly stronger than those with Mg, which clarifies that these nanostructures are appropriate as anodes of MIBs.

The E_{ad}, in kcal mol^{-1}, between Mg^{2+} and the nanotube showed the highest adsorption energy; the E_{ad} values changed in the order tube (−236.8) > cone (−192.8) > sheet (−176.1) > cage (−143.6). However, the cell voltage, V_{cell}, was the highest for the nanocone. The changes in V_{cell} of the MIBs are in the order cone (−4.14 V) > tube (−3.84 V) > sheet (−3.76 V) > cage (−3.09 V). The interactions between Mg^{2+} and Mg and the nanostructures play remarkable roles in the determination of the cell voltage. The strong interaction between Mg^{2+} and the nanostructures and the weak interaction between Mg and the nanostructures led to high V_{cell} values. In a comparison between the nanotube and nanocone, strong interactions between Mg and the nanotube led to a decreased V_{cell} of the nanotube with respect to that of the nanocone.

This study confirms that the advantages of Mg, including its low cost and availability, combined with its high V_{cell} value are of benefit to the battery scientists to study MIBs-nanostructures after overcoming technical issues.

Conflicts of interest

There are no conflicts to declare.

Acknowledgements

The authors wish to acknowledge to “Instituto de Quimica and Medica (CSIC)” for their support of this research.

References

1 W. Xu, J. Wang, F. Ding, X. Chen, E. Nasybulin, Y. Zhang and J.-G. Zhang, *Energy Environ. Sci.*, 2014, **7**, 513–537.
2 S. W. Kim, D. H. Seo, X. Ma, G. Ceder and K. Kang, *Adv. Energy Mater.*, 2012, **2**, 710–721.
3 P. Novak, R. Imhof and O. Haas, *Electrochim. Acta*, 1999, **45**, 351–367.
4 D. Aurbach, Y. Gofer, Z. Lu, A. Schechter, O. Chusid, H. Gizbar, Y. Cohen, V. Ashkenazi, M. Moshkovich and R. Turgeman, *J. Power Sources*, 2001, **97**, 28–32.
5 D. Aurbach, Z. Lu, A. Schechter and Y. Gofer, *Nature*, 2000, **407**, 724.
6 M. M. Huie, D. C. Bock, E. S. Takeuchi, A. C. Marschilok and K. J. Takeuchi, *Coord. Chem. Rev.*, 2015, **287**, 15–27.
7 R. Zhang, X. Yu, K.-W. Nam, C. Ling, T. S. Arthur, W. Song, A. M. Knapp, S. N. Ehrlich, X.-Q. Yang and M. Matsui, *Electrochem. Commun.*, 2012, **23**, 110–113.
8 Z. Tao, L. Xu, X. Gou, J. Chen and H. Yuan, *Chem. Commun.*, 2004, **40**, 2080–2081.
9 X. Han, C. Liu, J. Sun, A. D. Sendek and W. Yang, *RSC Adv.*, 2018, **8**, 7196.
10 A. O. Pereira and C. R. Miranda, *J. Phys. Chem. C*, 2015, **119**, 4302–4311.
11 (*a*) S. A. Siadati, E. Vessally, A. Hosseinian and L. Edjlali, *Synth. Met.*, 2016, **220**, 606–611; (*b*) R. Rostamoghli, M. Vakili, A. Banaei, E. Pourbashir and K. Jalalierad, *Chem. Rev. Lett.*, 2018, **1**, 31–36; (*c*) M. Heidari Nezhad Janjanpour, M. Vakili, S. Daneshmehr, K. Jalalierad and F. Alipour, *Chem. Rev. Lett.*, 2018, **1**, 45–49.
12 S. A. Siadati, E. Vessally, A. Hosseinian and L. Edjlali, *Talanta*, 2017, **162**, 505–510.
13 E. Vessally, S. Soleimani–Amiri, A. Hosseinian, L. Edjlal and A. Bekhradnia, *Phys. E*, 2017, **87**, 308–311.
14 A. Hosseinian, E. Saedi Khosroshahi, K. Nejati, E. Edjlali and E. Vessally, *J. Mol. Model.*, 2017, **23**, 354.
15 K. Nejati, A. Hosseinian, L. Edjlali and E. Vessally, *J. Mol. Liq.*, 2017, **229**, 167–171.
16 P. Subalakshmi and A. Sivashanmugam, *J. Alloys Compd.*, 2017, **690**, 523–531.
17 K. Nejati, A. Hosseinian, A. Bekhradnia, E. Vessally and L. Edjlal, *J. Mol. Graphics Modell.*, 2017, **74**, 1–7.
18 M. Li, Y.-J. Liu, J.-x. Zhao and X.-g. Wang, *Appl. Surf. Sci.*, 2015, **345**, 337–343.
19 Y. Xing, Z. Xi, Z. Xue, X. Zhang, J. Song, R. Wang, J. Xu, Y. Song, S. Zhang and D. Yu, *Appl. Phys. Lett.*, 2003, **83**, 1689–1691.

20 M. Nayebzadeh, A. A. Peyghan and H. Soleymanabadi, *Phys. E*, 2014, **62**, 48–54.
21 J.-D. Chai and M. Head-Gordon, *Phys. Chem. Chem. Phys.*, 2008, **10**, 6615.
22 U. Salzner and A. Aydin, *J. Chem. Theory Comput.*, 2011, **7**, 2568–2583.
23 M. J. Frisch, G. W. Trucks, H. B. Schlegel, G. E. Scuseria, M. A. Robb, J. R. Cheeseman, G. Scalmani, V. Barone, B. Mennucci, G. A. Petersson, H. Nakatsuji, M. Caricato, X. Li,H. P. Hratchian, A. F. Izmaylov, J. Bloino, G. Zheng, J. L. Sonnenberg,M. Hada, M. Ehara, K. Toyota, R. Fukuda, J. Hasegawa, M. Ishida, T. Nakajima, Y. Honda, O. Kitao, H. Nakai, T. Vreven, J. A. Montgomery Jr, J. E. Peralta, F. Ogliaro, M. J. Bearpark, J. Heyd, E. N. Brothers, K. N. Kudin, V. N. Staroverov, R. Kobayashi, J. Normand, K. Raghavachari, A. P. Rendell, J. C. Burant, S. S. Iyengar, J. Tomasi, M. Cossi, N. Rega, N. J. Millam, M. Klene, J. E. Knox, J. B. Cross, V. Bakken, C. Adamo, J. Jaramillo, R. Gomperts, R. E. Stratmann, O. Yazyev, A. J. Austin, R. Cammi, C. Pomelli, J. W. Ochterski, R. L. Martin, K. Morokuma, V. G. Zakrzewski, G. A. Voth, P. Salvador, J. J. Dannenberg, S. Dapprich, A. D. Daniels, O. Farkas, J. B. Foresman, J. V. Ortiz, J. Cioslowski and D. J. Fox, *Gaussian09 program*, Gaussian Inc., Wallingford, CT, 2009.
24 S. Grimme, *J. Comput. Chem.*, 2004, **25**, 1463–1473.
25 S. F. Boys and F. Bernardi, *Mol. Phys.*, 1970, **19**, 553–561.
26 N. O'Boyle, A. Tenderholt and K. Langner, *J. Comput. Chem.*, 2018, **29**, 839–845.
27 H. F. Dos Santos, L. A. De Souza, W. B. D. Almeida and T. Heine, *J. Phys. Chem. C*, 2014, **118**, 24761–24768.
28 R. F. W. Bader, in *Atoms in Molecules: A Quantum Theory*, ed. J. Halpen and M. L. H. Green, The international series of monographs of chemistry, Clarendon Press, Oxford, 1990.
29 P. A. Denis and F. Iribarne, *Chem. Phys. Lett.*, 2013, **573**, 15–18.
30 D. Datta, J. Li and V. B. Shenoy, *ACS Appl. Mater. Interfaces*, 2014, **6**, 1788–1795.
31 Z. Gao, C. S. Chin, J. H. K. Chiew and J. J. C. Zhang, *Energies*, 2017, **10**, 1503.
32 F. Gharibzadeh, S. Gohari, K. Nejati, B. Hashemzadeh and S. Mohammadiyan, *Chem. Rev. Lett.*, 2018, **1**, 16–22.
33 I. Torkpoor, M. Heidari Nezhad Janjanpour, N. Salehi, F. Gharibzadeh and L. Edjlali, *Chem. Rev. lett.*, 2018, **1**, 2–8.